Available online at www.sciencedirect.com
SCIENCE DIRECT®
Bioorganic & Medicinal Chemistry 12 (2004) 6085–6095
Bioorganic & Medicinal Chemistry

Flexible docking of pyridinone derivatives into the non-nucleoside inhibitor binding site of HIV-1 reverse transcriptase☆

José Luis Medina-Franco,[a] Sergio Rodríguez-Morales,[a] Cecilia Juárez-Gordiano,[a] Alicia Hernández-Campos,[a] Jesús Jiménez-Barbero[b,*] and Rafael Castillo[a,*]

[a]*Departamento de Farmacia, Facultad de Química, UNAM, CU, DF 04510, Mexico*
[b]*Centro de Investigaciones Biológicas, CSIC, Madrid 28040, Spain*

Received 26 February 2004; revised 3 September 2004; accepted 8 September 2004
Available online 2 October 2004

Abstract—Potent non-nucleoside reverse transcriptase inhibitors (NNRTIs) of the pyridinone derivative type were docked into nine NNRTIs binding pockets of HIV-1 reverse transcriptase (RT) structures. The docking results indicate that pyridinone analogues adopt a butterfly conformation and share the same binding mode as the crystal inhibitors in the pocket geometries of nevirapine, 1051U91, 9-Cl-TIBO, Cl-α-APA, efavirenz, UC-781, and S-1153. The results are in agreement with the data concerning mutational and structure–activity relationships available for pyridinone analogues and aid in the understanding, at the molecular level, of the biological response of published hybrid pyridinone molecules. Strategies to design further pyridinone derivatives active against RT containing mutations are discussed.

1. Introduction

The reverse transcriptase (RT) of the human immunodeficiency virus type 1 (HIV-1) is an attractive target in the treatment of the acquired immune deficiency syndrome (AIDS), for which no completely successful chemotherapy is yet available.[1,2] RT inhibitors are classified as nucleoside and non-nucleoside, depending on their action mechanism. One advantage of the latter group is that they lack the toxic effects associated with the former. To date, three non-nucleoside RT inhibitors have been approved for clinical use named nevirapine (VIRAMUNE®), delavirdine (RESCRIPTOR®), and efavirenz (SUSTIVA®),[1] however, all these and other approved drugs induce drug resistant variants of HIV-1.

Pyridinone derivatives[3] are a class of non-nucleoside reverse transcriptase inhibitors (NNRTIs). From kinetic[3] and analysis of resistance mutations[4] it was concluded that this type of inhibitors should bind in the same pocket as other NNRTIs. Extensive structure–activity relationship (SAR) studies have been conducted for these compounds leading to potent RT inhibitors (Fig. 1).[5–8]

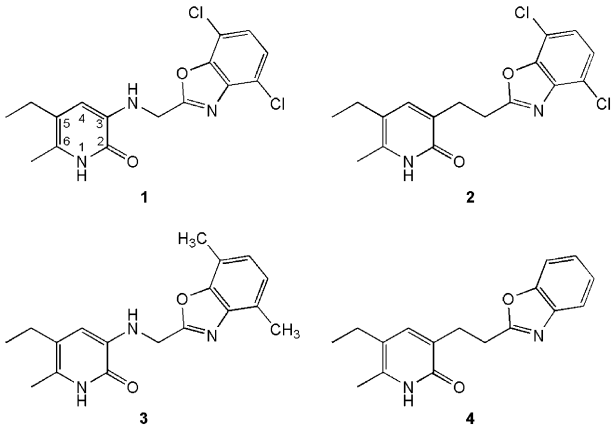

Figure 1. Pyridinone derivatives studied.

Keywords: AutoDock; Binding mode model; Mutation; Non-nucleoside reverse transcriptase inhibitors.
☆Taken in part from the Ph.D. dissertation of José Luis Medina-Franco.
* Corresponding authors. Tel./fax: +52 5622 5287 (R.C.); tel.: +34 91534 6623; fax: +34 91564 4853 (J.J.); e-mail addresses: jjbarbero@cib.csic.es; rafaelc@servidor.unam.mx

0968-0896/$ - see front matter © 2004 Elsevier Ltd. All rights reserved.
doi:10.1016/j.bmc.2004.09.008

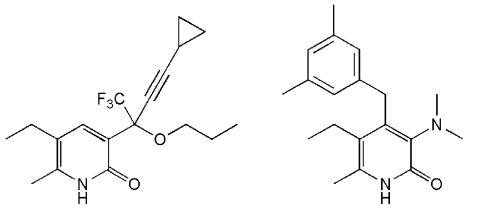

Figure 2. Hybrid pyridinone analogues with anti-HIV-1 RT inhibitory activity.

Compound **1** was subject to clinical studies, which showed good activity in patients, but rapid resistant strains of the virus emerged.[9,10] Amino acid substitutions mainly at positions 103 and 181 are responsible for the emergence of resistant virus not only for **1** but also for other pyridinone derivatives.[10–12]

Several quantitative structure–activity relationship analyses (QSAR)[13,14] have been performed for pyridinone analogues in which a hydrophobic character of the binding pocket appears. Recent hybrid pyridinone–NNRTIs designs have generated molecules with RT inhibitory activity against wild type and mutant strains (Figs. 2 and 3).[15–17] This suggests the importance of the pyridinone ring for RT inhibitory activity and demonstrates how the pyridinone ring can lead to active compounds against mutant strains; however, in these studies[15–17] an explanation for the activity of the hybrid pyridinone inhibitors against the mutant strains at the molecular level is not provided.

Studies of several crystal structures of HIV-1 RT in the apo form[18] and complexed with different NNRTIs have been published.[19–30] The non-nucleoside inhibitor binding pocket of HIV-1 RT is formed by the amino acids Pro95, Leu100, Lys101, Lys103, Val106, Val179, Tyr181, Tyr188, Gly190, Phe227, Trp229, Leu234, His235, Pro236, and Tyr318 of the p66 subunit and Glu138 of the p51 subunit. Crystal structures of RT–NNRTIs complexes reveal that some amino acids of the binding pocket adopt different conformations when bound to different inhibitors leading to distinct pocket volumes.[20,24,27] A marked variation in the pocket geometry is due to the modified position of the amino acid Pro236 when RT is complexed with 1-[(2-hydroxyethoxy)-methyl]-6-(phenylthio)thymine (HEPT) derivatives.[20] Despite these variations, several NNRTIs share a common binding mode, which is a butterfly-like conformation,[19–23,25,26,28,29] however, no crystal structures of HIV-1 RT in complex with pyridinone analogues that explain the resistance of HIV-1 RT to pyridinone analogues are available.

In order to gain an insight into the binding mode and interactions of pyridinone derivatives with HIV-1 RT and, consequently, to improve the development of more efficient HIV-1 RT inhibitors, especially active against mutant strains, we hereby describe a study of the docking of potent pyridinone derivatives (Fig. 1) with HIV-1 RT. The docking studies will provide information for a better understanding of drug resistant mechanisms. The compounds were flexibly docked with the program AutoDock 3.0[31] into several crystal structures of RT complexed with structural diverse NNRTIs. Since no crystal structure is available for RT in complex with

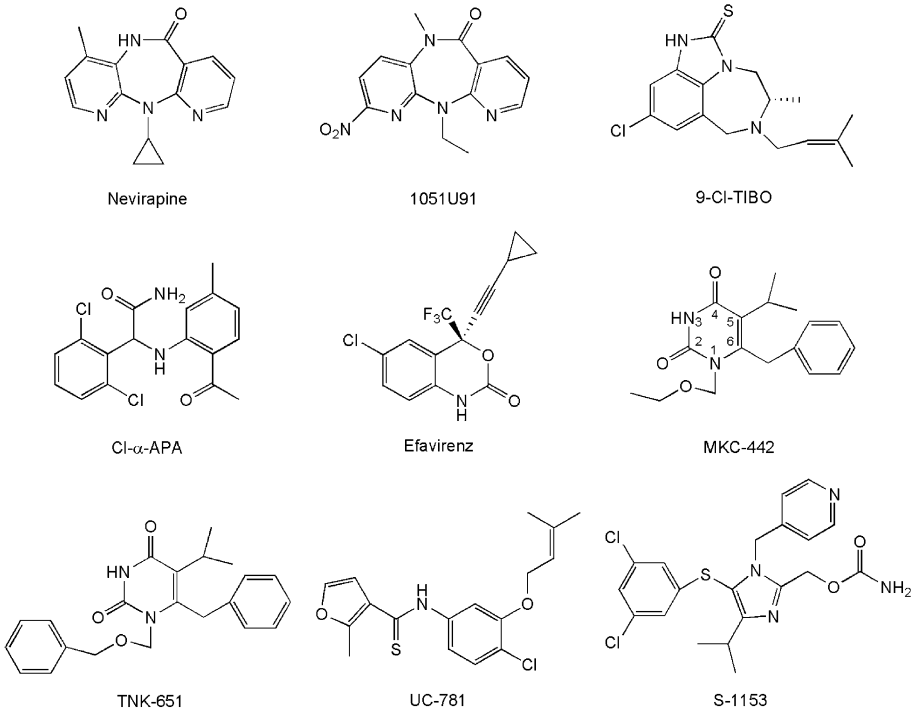

Figure 3. NNRTIs found in the crystal HIV-1 RT complexes.

pyridinones, computational docking is a useful tool to develop models that will assist in the rational design of further inhibitors. Previous docking studies with other NNRTIs have been conducted.[32–36] Using different pocket geometries is a good approach to model the flexible binding site.[32,37,38]

2. Results

Crystal HIV-1 RT structures complexed with the NNRTIs nevirapine, 1051U91, 9-Cl-TIBO, Cl-α-APA, efavirenz, MKC-442, TNK-651, UC-781, and S-1153 were used (Fig. 3). Table 1 provides a summary of the data and source of these structures.

2.1. Validation of the docking protocol

The docking protocol was validated for each crystal structure predicting the binding mode of the corresponding inhibitor. Each NNRTI was removed from the active site and docked back into the binding pocket in the conformation found in the crystal structure. The results of the validation are summarized in Table 2.

AutoDock successfully predicted the binding mode of the crystal NNRTIs with RMS deviations below or near 1 Å. The highly-populated clusters obtained in most cases indicate that the docking program found one binding mode mainly.

Table 1. Crystal HIV-1 RT structures used in this study

NNRTI	PDB code	Resolution Å	*R*-factor	Reference
Nevirapine	1VRT	2.2	0.186	19
1051U91	1RTH	2.2	0.214	19
9-Cl-TIBO	1REV	2.6	0.224	21
Cl-α-APA	1VRU	2.4	0.187	19
Efavirenz	1FK9	2.5	0.218	22
MKC-442	1RT1	2.55	0.197	20
TNK-651	1RT2	2.55	0.207	20
UC-781	1RT4	2.90	0.237	29
S-1153	1EP4	2.50	0.254	23

Table 2. Docking of crystal NNRTIs

NNRTI	Members in cluster[a]	Lowest energy (kcal/mol)[b]	Average energy (kcal/mol)	RMSD (Å)
Nevirapine	100	−9.68	−9.67	0.70
1051U91	100	−9.97	−9.95	1.25
9-Cl-TIBO	100	−11.83	−11.82	0.89
Cl-α-APA	68	−10.49	−10.31	0.96
Efavirenz	99	−10.97	−10.96	0.24
MKC-442	97	−11.15	−11.05	0.75
TNK-651	88	−14.01	−13.82	0.46
UC-781	93	−12.38	−12.03	0.92
S-1153	59	−15.63	−15.30	0.54

[a] The first cluster of a total 100 runs is shown.
[b] Value for the optimal structure in the cluster. Docking energies are as

2.2. Docking of pyridinone derivatives

The top ranked binding conformation found for each compound in the binding pocket of nevirapine was docked into the binding pockets of the other eight NNRTIs. The results are summarized in Table 3. Since the different binding sites were superimposed onto the structure of the RT–nevirapine complex before docking (see Section 5 for details), the RMSD values in Table 3 are an approximation of the similarity between the conformation found for each compound within a binding pocket and the pocket of nevirapine. According to the most populated clusters, **1**–**4** occupy the same binding pocket as the corresponding NNRTI and have the same orientation as nevirapine, 1051U91, 9-Cl-TIBO, Cl-α-APA, efavirenz, UC-781, and S-1153. In the pockets of nevirapine and Cl-α-APA, the most populated cluster for each compound also showed the lowest average docked energy (Figs. 4 and 5).

In the binding pockets of MKC-442 and TNK-651 (HEPT derivatives) it was predicted that the pyridinone analogues would have a different binding mode from that of the crystal inhibitor. In these pockets, the benzoxazol ring of the pyridinone derivatives is located in the same sub-pocket volume as the ethoxymethyl group of MKC-442 and the (benzyloxy)methyl group of TNK-651 (Figs. 6 and 7). In all binding pockets it was predicted that the docked pyridinone molecule would have a butterfly-like geometry.

For the binding pockets of nevirapine, 1051U91, 9-Cl-TIBO, Cl-α-APA, efavirenz, UC-781, and S-1153 a very good agreement between the docking energies calculated by AutoDock and the biological activity was observed. Table 4 summarizes the IC_{50} reported for **1**–**4**[3] and the average of docking energies estimated within the seven binding pockets. This good relationship is an indication that the docking calculation produced reasonable binding modes within these binding geometries. For the binding pockets of MKC-442 and TNK-651 no good agreement between the biological activity[3] and the docking energies (Table 3) was observed.

After docking, the binding pocket of nevirapine in complex with the top ranked binding conformation of **1**–**4** was fully optimized.[39] Very small variations were observed between the conformations predicted by AutoDock and the conformations of **1**–**4** after minimization.

3. Discussion

3.1. Docking model

The docking results indicate that the pyridinone derivatives have a common binding mode in the binding pockets of nevirapine, 1051U91, 9-Cl-TIBO, Cl-α-APA, efavirenz, UC-781, and S-1153. The hydrophobic character of the binding pocket is in very good agreement with the QSAR data available for pyridinone derivatives.[13,14] The pyridinone molecules adopt a

Table 3. Docking of **1**–**6** into different binding pockets

Binding pocket	Compound	Cluster[a]	Members in cluster	Lowest energy (kcal/mol)[b]	Average energy (kcal/mol)	RMSD (Å)[c]
Nevirapine	**1**	1	92	−11.13	−11.08	0.00
	2	1	93	−11.69	−11.64	0.00
	3	1	94	−11.18	−11.14	0.00
	4	1	96	−10.63	−10.58	0.00
	5	1	100	−9.67	−9.53	0.40
	6	1	3	−10.62	−10.60	3.10
	6	2	92	−10.51	−10.49	0.15
1051U91	**1**	1	91	−10.90	−10.81	0.33
	2	1	99	−11.73	−11.70	0.55
	3	1	93	−10.97	−10.89	0.34
	4	1	3	−10.85	−10.74	2.65
	4	2	89	−10.58	−10.45	1.08
	5	1	96	−9.42	−9.22	0.70
	6	1	96	−10.42	−10.39	0.59
9-Cl-TIBO	**1**	1	3	−11.50	−11.40	3.01
	1	4	49	−11.08	−10.90	0.75
	2	1	93	−12.12	−11.75	1.07
	3	1	3	−11.47	−11.37	2.95
	3	6	65	−11.13	−10.98	0.74
	4	1	97	−11.23	−11.13	0.78
	5	1	100	−10.15	−9.96	0.62
	6	1	5	−10.37	−10.32	1.88
	6	2	73	−10.35	−10.27	1.04
Cl-α-APA	**1**	1	92	−10.96	−10.82	0.68
	2	1	94	−11.65	−11.53	0.62
	3	1	96	−11.02	−10.91	0.67
	4	1	95	−10.68	−10.56	0.63
	5	1	91	−9.32	−9.12	0.55
	6	1	4	−10.07	−10.03	1.68
	6	2	94	−9.90	−9.88	0.35
Efavirenz	**1**	1	10	−11.49	−11.25	1.47
	1	2	74	−11.47	−11.26	0.56
	2	1	84	−11.95	−11.84	0.63
	3	1	75	−11.57	−11.39	0.60
	4	1	80	−11.12	−10.97	0.53
	5	1	83	−10.42	−10.18	0.67
	6	1	15	−10.75	−10.54	2.91
	6	3	40	−10.43	−10.28	2.43
MKC-442	**1**	1	24	−11.76	−11.66	3.18
	2	1	4	−12.09	−12.05	3.06
	2	2	35	−12.04	−11.99	2.89
	3	1	25	−11.80	−11.72	3.15
	4	1	5	−11.21	−11.00	3.29
	4	9	59	−10.66	−10.60	0.59
	5	1	79	−9.56	−9.34	1.41
	6	1	97	−11.01	−10.99	0.72
TNK-651	**1**	1	1	−11.84	−11.84	3.88
	1	2	32	−11.71	−11.66	3.03
	2	1	4	−12.49	−12.29	3.52
	2	2	34	−12.19	−12.13	2.87
	3	1	3	−12.28	−12.19	3.63
	3	2	34	−11.76	−11.71	2.97
	4	1	3	−11.74	−11.53	3.39
	4	8	29	−10.89	−10.82	2.76
	5	1	98	−9.95	−9.61	0.96
	6	1	96	−11.00	−10.98	0.66
UC-781	**1**	1	16	−11.39	−11.21	3.15
	1	4	67	−10.60	−10.54	0.68
	2	1	15	−12.05	−11.88	2.78
	2	2	75	−11.46	−11.38	0.74
	3	1	13	−11.41	−11.14	3.15
	3	3	78	−10.82	−10.77	0.79

Table 3 (*continued*)

Binding pocket	Compound	Cluster[a]	Members in cluster	Lowest energy (kcal/mol)[b]	Average energy (kcal/mol)	RMSD (Å)[c]
	4	1	2	−10.76	−10.49	2.87
	4	2	93	−10.73	−10.67	0.62
	5	1	56	−9.84	−9.57	1.20
	5	2	38	−9.67	−9.41	1.24
	6	1	96	−10.65	−10.61	1.02
S-1153	**1**	1	2	−10.93	−10.91	3.08
	1	3	71	−10.76	−10.62	1.22
	2	1	73	−11.30	−11.10	1.34
	3	1	3	−10.90	−10.83	3.65
	3	2	88	−10.77	−10.70	1.37
	4	1	18	−10.41	−10.27	3.69
	4	9	53	−10.03	−9.98	1.14
	5	1	37	−8.99	−8.76	1.28
	6	1	99	−10.07	−10.05	0.56

[a] The best clusters of a total 100 runs are shown.
[b] Value for the optimal structure in the cluster. Docking energies are as determined by AutoDock.
[c] Coordinates found with the docking into the nevirapine binding pocket were used as reference.

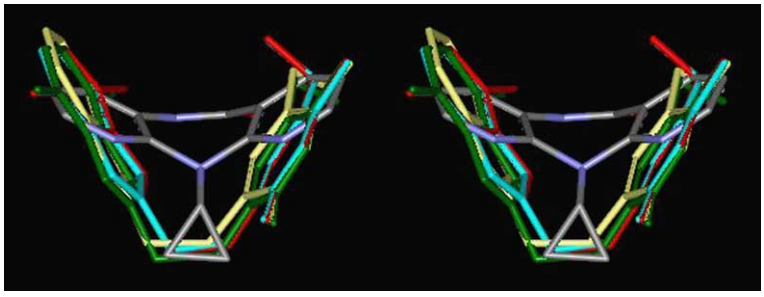

Figure 4. Top ranked binding mode of **1** (red), **2** (green), **3** (blue), and **4** (yellow) into the binding site of nevirapine. Nevirapine (colored by atom type) is displayed for comparison. Hydrogens are omitted for clarity.

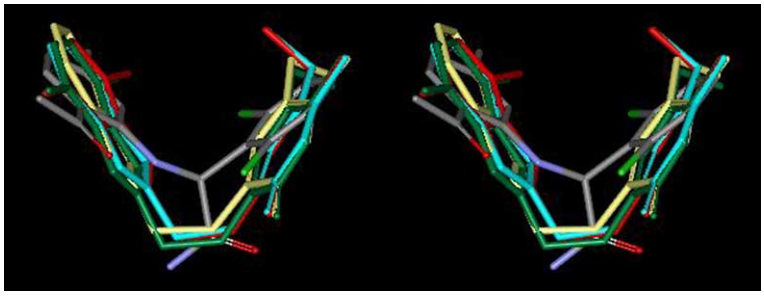

Figure 5. Top ranked binding mode of **1**–**4** into the binding site of Cl-α-APA (displayed for comparison). The color scheme is that of Figure 4. Hydrogens are omitted for clarity.

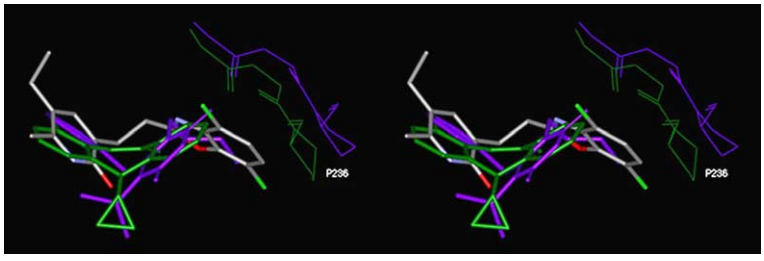

Figure 6. Top ranked binding mode of **2** (colored by atom type) into the binding site of MKC-442 (thick purple sticks). The position of Pro236 is displayed when MKC-442 (thin purple sticks) and nevirapine (thin green sticks) are the crystal inhibitors. Nevirapine is in thick green sticks. Hydrogens are omitted for clarity.

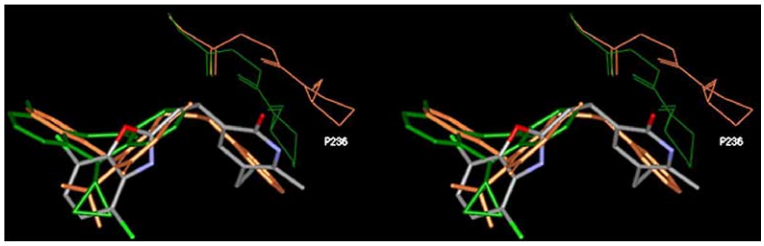

Figure 7. Top ranked binding mode of **2** (colored by atom type) into the binding site of TNK-651 (thick orange sticks). The position of Pro236 is displayed when TNK-651 (thin orange sticks) and nevirapine (thin green sticks) are the crystal inhibitors. Nevirapine is in thick green sticks. Hydrogens are omitted for clarity.

Table 4. Comparison between the docking energy and biological activity

Compound	IC_{50} (nM)	Docking energy (kcal/mol)[a]
1	19	−10.99
2	9.6	−11.70
3	20	−11.07
4	22	−10.71

[a] Average of docking energies of the optimal structure in the most populated clusters obtained within the binding sites of nevirapine, 1051U91, 9-Cl-TIBO, Cl-α-APA, efavirenz, UC-781, and S-1153.

butterfly-like conformation and may be roughly overlapped with the crystal structures of the NNRTIs (Figs. 4 and 5). Similar results have been obtained for other NNRTIs for which no crystal structures of the complex are available.[34] A butterfly-like shape has also been calculated to be the most stable for several pyridinone analogues in the unliganded state based on ab-inito methods.[40]

According to the optimized RT–pyridinone complexes, the residues Pro95, Leu100, Try181, and Tyr188 form the binding pocket of the benzoxazol ring. The amino acids Lys101, Lys103, His235, and Tyr318 form the pocket of the pyridinone ring. A hydrogen bond between the polar proton of the pyridinone ring and the main-chain carbonyl oxygen of Lys101 may be formed (Fig. 8). A similar hydrogen bond to the main-chain carbonyl oxygen of Lys101 is observed for several other NNRTIs.[20–22,25–27,29,30] The hydrophobic contacts between the aromatic ring of Tyr181 and the benzoxazol ring of the pyridinone derivative may stabilize the complex and also be responsible for the decrease of activity upon the mutation of this residue.[11,12] Similar interactions are observed between one of the aromatic rings of other NNRTIs and Tyr181.[41] The hydrophobic contacts with Lys103 may also explain the decrease of potency of pyridinone derivatives when the mutation of this amino acid occurs.[12]

A further interesting feature of the docking model is the region surrounding the linker between the aromatic rings of the pyridinone analogues. The linker occupies the same sub-pocket volume as the cyclopropyl group of nevirapine, the amide group of Cl-α-APA, the trifluoromethyl group of efavirenz, the methylfuran-3-carbothioamide group of UC-781 and the isopropyl group of S-1153 (Figs. 4 and 5. See also Figs. 9, 13, 15), the ethyl group of 1051U91 and the 5(*S*)-methyl group of 9-Cl-TIBO. These structural relationships among several NNRTIs have been previously quoted.[20] It is interesting to note that though the chemical structures of these groups are different they all seem to play a steric role,[20] which is in full agreement with the SAR data of pyridinone analogues. Moreover, in the QSAR studies of pyridinones no significant difference was found between and ethyl or aminomethylene as linkers on the inhibitory potency.[13]

AutoDock predicted a different binding mode for the pyridinone analogues in the pocket geometries of

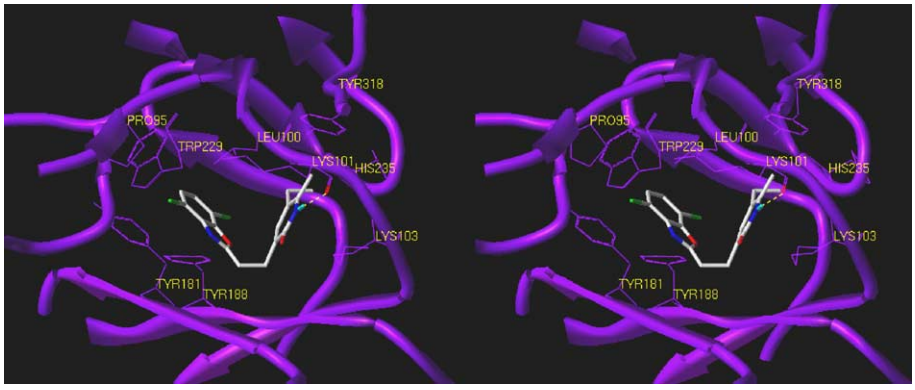

Figure 8. RT–**2** complex. Optimized complex of **2** into the binding pocket of nevirapine is shown. The hydrogen bond is displayed as yellow dashes. Amino acids within 3.6 Å of the benzoxazol and pyridinone ring are labeled. Trp229 is also labeled for reference. Hydrogens are omitted.

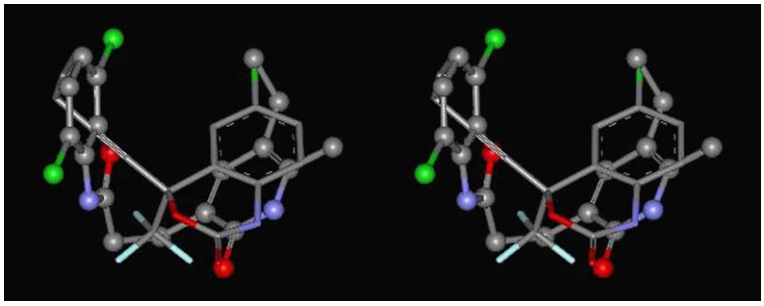

Figure 9. Top ranked binding mode of **2** (ball and sticks) into the binding site of efavirenz. Efavirenz (sticks) is displayed for comparison. Hydrogens are omitted for clarity.

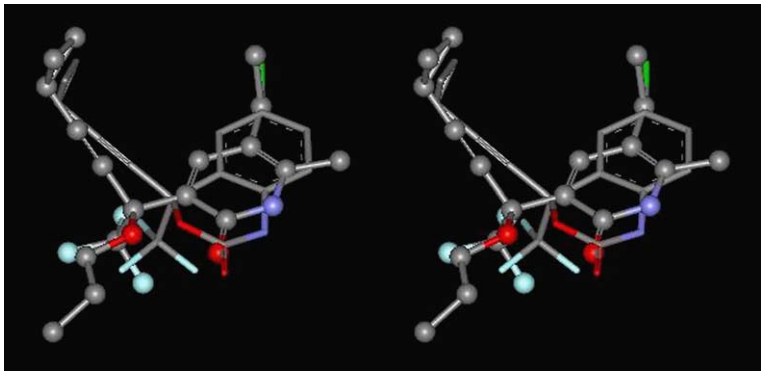

Figure 10. Top ranked binding mode of the hybrid pyridinone–efavirenz (**5**) (ball and sticks) into the binding site of efavirenz. Efavirenz (sticks) is displayed for comparison. Hydrogens are omitted for clarity.

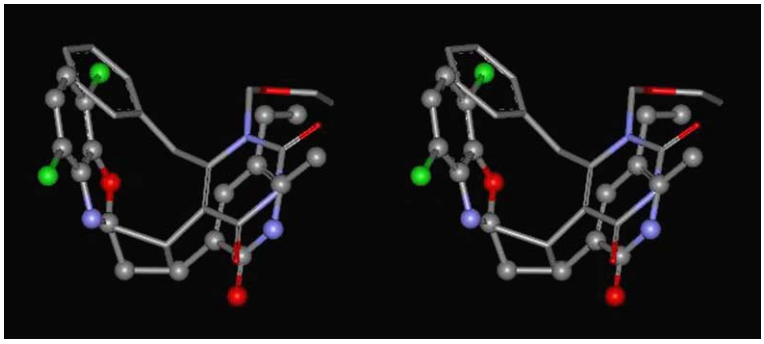

Figure 11. Top ranked binding mode of **2** (ball and sticks) found within the binding site of nevirapine compared with the binding mode of MKC-442 (sticks). Hydrogens are omitted for clarity.

MKC-442 and TNK-651. In these pockets, one of the aromatic rings of the pyridinone analogues roughly occupies the same sub-pocket volume as the N-1 substituent of these HEPT derivatives (Figs. 6 and 7). The different binding orientations found within these pockets may be explained by the different pocket geometries. It has been described that in the crystal structures of HEPT derivatives, the N-1 substituent is a 'tail' of the inhibitor that causes the highly flexible Pro236 loop to have a conformation similar to that observed in the unliganded RT structure.[20] AutoDock found better interactions if one of the aromatic rings of the pyridinones occupies the sub-pocket volume generated as a consequence of the Pro236 loop position (Figs. 6 and 7).

Since pyridinone derivatives lack the 'tail' of HEPT derivatives to maintain the Pro236 loop in that characteristic conformation, the actual binding pocket of pyridinone derivatives might be more related to the pocket geometries of the other NNRTIs studied. Moreover, for the binding pockets of MKC-442 and TNK-651 a good relationship between the docking energies (Table 3) and the biological activity[3] was not observed.

3.2. Understanding at the molecular level hybrid pyridinone–NNRTIs designs

Comparing the docked conformations of pyridinone derivatives in the pocket of efavirenz with the position

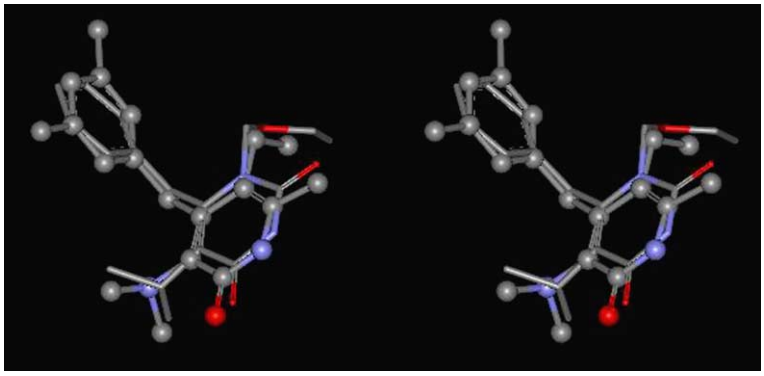

Figure 12. Top ranked binding mode of the hybrid pyridinone–MKC-442 molecule (**6**) (balls and sticks) into the binding site of MKC-442. MKC-442 (sticks) is displayed for comparison. Hydrogens are omitted for clarity.

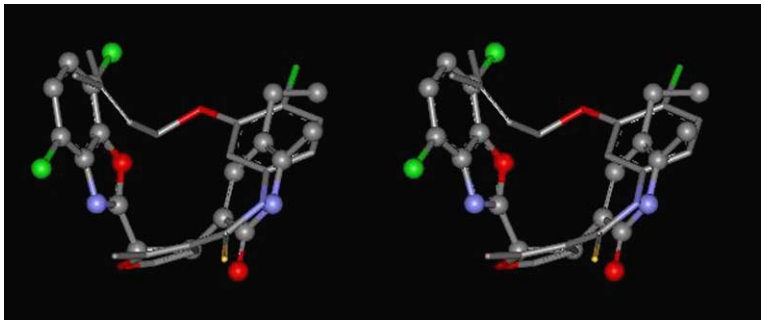

Figure 13. Top ranked binding mode of the most populated cluster of **2** (ball and sticks) into the binding site of UC-781. UC-781 (sticks) is displayed for comparison. Hydrogens are omitted for clarity.

of efavirenz found within the crystal, it is observed that the benzoxazol ring of pyridinones overlaps the cyclopropyl-propynyl group of efavirenz (Fig. 9). A close comparison of the binding modes of pyridinones and efavirenz helps to understand at the molecular level the strategy of substituting the pyridinone ring at position 4 with a cyclopropyl-propynyl group to generate an active compound (**5**).[17] In order to test this hypothesis the pyridinone–efavirenz hybrid molecule (**5**) was flexibly docked into several pocket geometries. Docking results are in Table 3. In the binding pocket of efavirenz, and in most binding geometries, the top ranked binding conformation showed the expected conformation and position with a butterfly-like conformation. The cyclopropyl-propynyl groups of the hybrid molecule and efavirenz overlap, besides, the pyridinone ring of the hybrid overlaps the benzoxazin-2-one ring of efavirenz (Fig. 10).

When the binding mode of pyridinone derivatives found within the pocket geometries of nevirapine, 1051U91, 9-Cl-TIBO, Cl-α-APA, efavirenz, UC-781, and S-1153 was compared with the binding modes of MKC-442 and TNK-651 it was observed that the pyridinone ring overlaps the uracil ring of these HEPT derivatives (Fig. 11). The linker of pyridinones occupies the same sub-pocket volume as the isopropyl group of MKC-442 and TNK-651. Also, the benzoxazol ring of pyridinones is approximately in the same binding region as the benzyl group of the HEPT derivatives. These structural relationships aid in the understanding, at the molecular level, of several SAR results obtained for a series of published hybrid pyridinone–HEPT molecules.[15,16] The docking model totally agrees with the approach of substituting the pyridinone molecule at position 4 with a benzyl (Fig. 2) or phenylthio groups (Fig. 11). The docking of the hybrid pyridinone–MKC-442 molecule (**6**) into different pocket geometries shows that the hybrid molecule adopts the expected butterfly conformation (Fig. 12). The docking results are in Table 3.

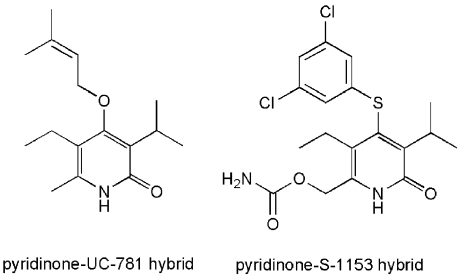

Figure 14. Examples of pyridinone derivatives with potential activity against RT containing the mutations Tyr181Cys (pyridinone–UC-781 hybrid) and Lys103Asn (pyridinone–S-1153 hybrid).

3.3. Strategies to design further pyridinone derivatives active against RT containing mutations

One major objective in the current design of NNRTIs is to develop compounds, which can inhibit mutant forms

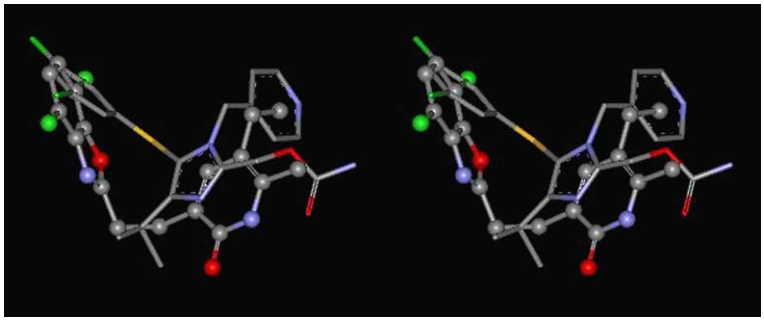

Figure 15. Top ranked binding mode of the most populated cluster of **2** (ball and sticks) into the binding site of S-1153. S-1153 (sticks) is displayed for comparison. Hydrogens are omitted for clarity.

of the enzyme. Some NNRTIs show greater resilience to drug resistance mutations within HIV-1 RT compared with first generation drugs such as nevirapine, 1051U91, and Cl-α-APA. Some of these compounds, so-called second-generation inhibitors, are efavirenz, UC-781, and S-1153.

It has been proposed that the main contribution to drug resistance for the Tyr181Cys mutation is the loss of aromatic ring stacking interactions between Tyr181 and an aromatic system, associated with a 'butterfly wing', of several NNRTIs.[42] A good example of such an aromatic system is the benzoxazol ring of pyridinone derivatives that makes contacts with Tyr181, however, in the case of UC-781, the (3-methylbut-2-enyl)oxy group makes fewer significant interactions with Tyr181 than an aromatic system and it is thought to be responsible for the activity of this compound against RT containing the single point mutation Tyr181Cys.[29] Comparing the binding mode of the top ranked conformation of **1**–**4** of the most populated cluster obtained within the pocket of UC-781 with the binding mode of UC-781 (Fig. 13) it is observed that the benzoxazol ring of the pyridinone derivatives may be replaced by a (3-methylbut-2-enyl)-oxy group. This may lead to pyridinones derivatives active against the RT containing the mutation Tyr181Cys. The (3-methylbut-2-enyl)oxy group can be at position 4 of the pyridinone ring. A dimethylamine or isopropyl group at position-3 can play the steric role of the ethylene or aminomethylene linker of pyridinone derivatives, as previously shown for **6** (Fig. 14).

The carbamate group of S-1153 has the ability to form an extensive net of hydrogen bonds with surrounding amino acids, thus making S-1153 active against RT containing the single point mutation Lys103Asn.[23] Comparing the top ranked conformation of **1**–**4** of the most populated cluster obtained within the binding pocket of S-1153 with the binding mode of the crystal inhibitor it is observed that the methyl group at the pyridinone ring shares the same sub-pocket volume as the carbamate group of S-1153 (Fig. 15). This observation suggests that substituting the position-6 of the pyridinone ring with a carbamate group or other group with the ability to form hydrogen bonds may lead to pyridinone derivatives active against RT containing the Lys103Asn mutation. The activity against RT containing the Tyr181Cys mutation may also be achieved by replacing the benzoxazol ring with a phenylthio or benzyl group *m*-substituted with methyl or chlorine groups. This strategy to overcome the Tyr181Cys mutation has already been successful for other NNRTIs.[15,16,43] Similar to the pyridinone–UC-781 design proposed above, a dimethylamine or isopropyl group at position 3 can play the steric role of the ethylene or aminomethylene linker.

The docking of the pyridinone–UC-781 and pyridinone–S-1153 hybrids in Figure 14 into several NNRTIs binding pockets shows that the hybrid molecule can adopt the expected conformation within these pockets. The proposed molecules represent potential alternatives to RT inhibitors that still present resistance issues in clinical studies. The modified pyridinones could be less toxic than some current second-generation inhibitors such as S-1153, which showed negative results in animal toxicity studies.[1] Also, the novel molecules will provide information for a better understanding of the drug resistant mechanisms and are examples of structure based designed compounds.

4. Conclusions

Automated flexible docking was used to study the binding mode of four pyridinone derivatives in the NNRTIs binding site. A single docking model was derived considering the pocket geometries of nevirapine, 1051U91, 9-Cl-TIBO, Cl-α-APA, efavirenz, UC-781, and S-1153. According to the docking model proposed, that agrees with the mutational and structure–activity relationship data available for pyridinone derivatives, the pyridinone analogues have a very similar binding mode to that of the crystallographic NNRTIs. The docking model helped to understand, at the molecular level, the biological activity reported for hybrid pyridinone–NNRTIs molecules. A different binding mode was predicted for the pyridinone derivatives within the pocket geometries of MKC-442 and TNK-651. The conformation of the Pro236 loop in these binding geometries, which is a consequence of the particular structure of HEPT derivatives, is thought to be the responsible to modify the docking predictions. Comparison of the predicted binding mode of pyridinone analogues with the actual binding mode of second generation NNRTIs suggests substitutions at the pyridinone ring that may lead to compounds active against RT containing mutations.

5. Experimental

Sybyl 6.8[44] was used for ligand and protein preparation. Molecular structure viewing was carried out with Sybyl 6.8 and Viewer Pro 4.2.[45] RT crystal structures were obtained from the Protein Data Bank.[46] Docking calculations were conducted with AutoDock 3.0.[31] In short, AutoDock performs an automated docking of the ligand with user-specified dihedral flexibility within a protein rigid binding site. The program performs several runs in each docking experiment. Each run provides one predicted binding mode.

All water molecules and magnesium ion, when present, were removed from the original Protein Data Bank files. The binding sites were separately superimposed before docking onto the structure of the RT–nevirapine complex, the structure with the highest resolution available, to compensate for differences in crystal form and domain orientations based on the 'core' of the p66 palm domain (residues 94–118, 156–215, and 225–243), residues 317–319 from the p66 connection domain, and residues 137–139 from the p51 fingers domain using Sybyl 6.8.

Polar hydrogen atoms were added and Kollman charges,[47] atomic solvation parameters and fragmental volumes were assigned to the protein. For validation of the docking protocol, ligand coordinates in the crystal complexes were removed and the bond orders were checked. The structure of 1051U91 in the PDB file 1RTH was corrected with Sybyl 6.8. For all ligands, Gasteiger charges[48] were assigned and non-polar hydrogen atoms merged. All torsions were allowed to rotate during docking.

The coordinates of the best docked conformation found for **1**–**4** within the pocket of nevirapine were used as starting coordinates to dock these compounds into the pockets of the other NNRTIs. To conduct docking validations the initial coordinates of NNRTIs were as found within the crystal.

The auxiliary program AutoGrid generated the grid maps. Each grid was centered at the crystal structure of the corresponding NNRTI. The grid dimensions were $23 \times 23 \times 23$ Å^3 with points separated by 0.375 Å. Lennard-Jones parameters 12–10 and 12–6, supplied with the program, were used for modeling H-bonds and van der Waals interactions, respectively. The distance-dependent dielectric permittivity of Mehler and Solmajer[49] was used for calculation of the electrostatic grid maps. For all ligands, random starting positions, random orientations, and torsions were used. The translation, quaternion, and torsion steps were taken from default values in AutoDock. The Lamarckian genetic algorithm and the pseudo-Solis and Wets methods were applied for minimization using default parameters. The number of docking runs was 100. The population in the genetic algorithm was 50, the energy evaluations were 250,000 and the maximum number of iterations 27,000.

After docking, the 100 solutions were clustered into groups with RMS deviations lower than 1.0 Å. The clusters were ranked by the lowest energy representative of each cluster.

In order to describe pyridinone-binding pocket interactions, the top ranked binding mode found by AutoDock for **1**–**4** in complex with the binding pocket of nevirapine was subject to full energy minimization utilizing Gasteiger-Hückel partial charges[50] and the Tripos force field[51] until the gradient of 0.05 kcal/mol was reached. During minimization, atoms within 6 Å from the ligand were free to move (other atoms were fixed).

Acknowledgements

J.L.M.-F. is grateful to CONACyT and DGAPA, UNAM, for the Ph.D. scholarships. We also would like to acknowledge CONACyT for financing project G-34851-M.

References and notes

1. De Clercq, E. *Int. J. Biochem. Cell Biol.* **2004**, *36*, 1800.
2. Jacobo-Molina, A.; Arnold, E. *Biochemistry* **1991**, *30*, 6351.
3. Goldman, M. E.; Nunberg, J. H.; O'Brien, J. A.; Quintero, J. C.; Schleif, W. A.; Freund, K. F.; Gaul, S. L.; Saari, W. S.; Wai, J. S.; Hoffman, J. M.; Anderson, P. S.; Hupe, D. J.; Emini, E. A.; Stern, A. M. *Proc. Natl. Acad. Sci. U.S.A.* **1991**, *88*, 6863.
4. Nunberg, J. H.; Schleif, W. A.; Boots, E. J.; O'Brien, J. A.; Quintero, J. C.; Hoffman, J. M.; Emini, E. A.; Goldman, M. E. *J. Virol.* **1991**, *65*, 4887.
5. Saari, W. S.; Hoffman, J. M.; Wai, J. S.; Fisher, T. E.; Rooney, C. S.; Smith, A. M.; Thomas, C. M.; Goldman, M. E.; O'Brien, J. A.; Nunberg, J. H.; Quintero, J. C.; Schleif, W. A.; Emini, E. A.; Stern, A. M.; Anderson, P. S. *J. Med. Chem.* **1991**, *34*, 2922.
6. Hoffman, J. M.; Wai, J. S.; Thomas, C. M.; Levin, R. B.; O'Brien, J. A.; Goldman, M. E. *J. Med. Chem.* **1992**, *35*, 3784.
7. Saari, W. S.; Wai, J. S.; Fisher, T. E.; Thomas, C. M.; Hoffman, J. M.; Rooney, C. S.; Smith, A. M.; Jones, J. H.; Bamberger, D. L.; Goldman, M. E.; O'Brien, J. A.; Nunberg, J. H.; Quintero, J. C.; Schleif, W. A.; Emini, E. A.; Anderson, P. S. *J. Med. Chem.* **1992**, *35*, 3792.
8. Hoffman, J. M.; Smith, A. M.; Rooney, C. S.; Fisher, T. E.; Wai, J. S.; Thomas, C. M.; Bamberger, D.; Barnes, J. L.; Williams, T. M.; Jones, J. H.; Olson, B. D.; O'Brien, J. A.; Goldman, M. E.; Nunberg, J. H.; Quintero, J. C.; Schleif, W. A.; Emini, E. A.; Anderson, P. S. *J. Med. Chem.* **1993**, *36*, 953.
9. Davey, R. T.; Dewar, R. L.; Reed, G. F.; Vasudevachari, M. B.; Polis, M. A.; Kovacs, J. A.; Fallon, J.; Walker, R. E.; Masur, H.; Haneiwich, S. E.; O'Neill, D. G.; Decker, M. R.; Metcalf, J. A.; Deloria, M. A.; Laskin, O. L.; Salzman, N.; Lane, H. C. *Proc. Natl. Acad. Sci. U.S.A.* **1993**, *90*, 5608.
10. Saag, M. S.; Emini, E. A.; Laskin, O. L.; Douglas, J.; Lapidus, W. I.; Schleif, W. A.; Whitley, R. J.; Hildebrand, C.; Byrnes, V. W.; Kappes, J. C.; Anderson, K. W.; Massari, F. E.; Shaw, G. M.; L-697,661 Working Group. *New Engl. J. Med.* **1993**, *329*, 1065.
11. Sardana, V. V.; Emini, E. A.; Gotlib, L.; Graham, D. J.; Lineberger, D. W.; Long, W. J.; Schlabach, A. J.;

Wolfgang, J. A.; Condra, J. H.. *J. Biol. Chem.* **1992**, *267*, 17526.
12. Byrnes, V. W.; Sardana, V. V.; Schleif, W. A.; Condra, J. H.; Waterbury, J. A.; Wolfgang, J. A.; Long, W. J.; Schneider, C. L.; Schlabach, A. J.; Wolanski, B. S.; Graham, D. J.; Gotlib, L.; Rhodes, A.; Titus, D. L.; Roth, E.; Blahy, O. M.; Quintero, J. C.; Staszewski, S.; Emini, E. A. *Antimicrob. Agents Chemother.* **1993**, *37*, 1576.
13. Garg, R.; Gupta, S. P.; Gao, H.; Babu, M. S.; Debnath, A. K.; Hansch, C. *Chem. Rev.* **1999**, *99*, 3525.
14. Gupta, S. P. In *Progress in Drug Research*; Jucker, E., Ed.; Birkhäuser: Basel, Switzerland, 2002; Vol. 58, pp 252–253.
15. Dollé, V.; Fan, E.; Nguyen, C. H.; Aubertin, A. M.; Kirn, A.; Andreola, M. L.; Jamieson, G.; Tarrago-Litvak, L.; Bisagni, E. *J. Med. Chem.* **1995**, *38*, 4679.
16. Dollé, V.; Nguyen, C. H.; Legraverend, M.; Aubertin, A. M.; Kirn, A.; Andreola, M. L.; Ventura, M.; Tarrago-Litvak, L.; Bisagni, E. *J. Med. Chem.* **2000**, *43*, 3949.
17. Corbett, J. W.; Kresge, K. J.; Pan, S.; Cordova, B. C.; Klabe, R. M.; Rodgers, J. D.; Erickson-Viitanem, S. K. *Bioorg. Med. Chem. Lett.* **2001**, *11*, 309.
18. Esnouf, R.; Ren, J.; Ross, C.; Jones, Y.; Stammers, D.; Stuart, D. *Nat. Struct. Biol.* **1995**, *2*, 303.
19. Ren, J.; Esnouf, R.; Garman, E.; Somers, D.; Ross, C.; Kirby, I.; Keeling, J.; Darby, G.; Jones, Y.; Stuart, D.; Stammers, D. *Nat. Struct. Biol.* **1995**, *2*, 293.
20. Hopkins, A. L.; Ren, J.; Esnouf, R. M.; Willcox, B. E.; Jones, E. Y.; Ross, C.; Miyasaka, T.; Walker, R. T.; Tanaka, H.; Stammers, D. K.; Stuart, D. I. *J. Med. Chem.* **1996**, *39*, 1589.
21. Ren, J.; Esnouf, R.; Hopkins, A.; Ross, C.; Jones, Y.; Stammers, D.; Stuart, D. *Structure* **1995**, *3*, 915.
22. Ren, J.; Milton, J.; Weaver, K. L.; Short, S. A.; Stuart, D. I.; Stammers, D. K. *Structure* **2000**, *8*, 1089.
23. Ren, J.; Nichols, C.; Bird, L. E.; Fujiwara, T.; Suginoto, H.; Stuart, D. I.; Stammers, D. K. *J. Biol. Chem.* **2000**, *275*, 14316.
24. Esnouf, R. M.; Ren, J.; Hopkins, A. L.; Ross, C. K.; Jones, E. Y.; Stammers, D. K.; Stuart, D. I. *Proc. Natl. Acad. Sci. U.S.A.* **1997**, *94*, 3984.
25. Ren, J.; Diprose, J.; Warren, J.; Esnouf, R. M.; Bird, L. E.; Ikemizu, S.; Slater, M.; Milton, J.; Balzarini, J.; Stuart, D. I.; Stammers, D. K. *J. Biol. Chem.* **2000**, *275*, 5633.
26. Chan, J. H.; Hong, J. S.; Hunter, R. N., III; Orr, G. F.; Cowan, J. R.; Sherman, D. B.; Sparks, S. M.; Reitter, B. E., III; Andrews, C. W., III; Hazen, R. J.; St Clair, M.; Boone, L. R.; Ferris, R. G.; Creech, K. L.; Roberts, G. B.; Short, S. A.; Weaver, K.; Ott, R. J.; Ren, J.; Hopkins, A.; Stuart, D. I.; Stammers, D. K. *J. Med. Chem.* **2001**, *44*, 1866.
27. Hsiou, Y.; Das, K.; Ding, J.; Clark, A. D., Jr.; Kleim, J. P.; Rosner, M.; Winkler, I.; Riess, G.; Hughes, S. H.; Arnold, E. *J. Mol. Biol.* **1998**, *284*, 313.
28. Ren, J.; Esnouf, R. M.; Hopkins, A. L.; Stuart, D. I.; Stammers, D. K. *J. Med. Chem.* **1999**, *42*, 3845.
29. Ren, J.; Esnouf, R. M.; Hopkins, A. L.; Warren, J.; Balzarini, J.; Stuart, D. I.; Stammers, D. K. *Biochemistry* **1998**, *37*, 14394.
30. Hogberg, M.; Sahlberg, C.; Engelhardt, P.; Noreen, R.; Kangasmetsa, J.; Johansson, N. G.; Oberg, B.; Vrang, L.; Zhang, H.; Sahlberg, B. L.; Unge, T.; Lovgren, S.; Fridborg, K.; Backbro, K. *J. Med. Chem.* **2000**, *43*, 304.
31. Morris, G. M.; Goodsell, D. S.; Halliday, R. S.; Huey, R.; Hart, W. E.; Belew, R. K.; Olson, A. J. *J. Comput. Chem.* **1998**, *19*, 1639.
32. Titmuss, S. J.; Keller, P. A.; Griffith, R. *Bioorg. Med. Chem.* **1999**, *7*, 1163.
33. Barreca, M. L.; Carotti, A.; Carrieri, A.; Chimiri, A.; Monforte, A. M.; Calace, M. P.; Rao, A. *Bioorg. Med. Chem.* **1999**, *7*, 2283.
34. Zhou, Z.; Madrid, M.; Madura, J. D. *Proteins* **2002**, *49*, 529.
35. Chen, H. F.; Yao, X. J.; Li, Q.; Yuan, S. G.; Panaye, A.; Doucet, J. P.; Fan, B. T. *SAR QSAR Environ. Res.* **2003**, *14*, 455.
36. Kontoyianni, M.; McClellan, L. M.; Sokol, G. S. *J. Med. Chem.* **2004**, *47*, 558.
37. Yadav, P. N. S.; Das, K.; Ding, J.; Arnold, E.; Yadav, J. S.; Modak, M. J. *J. Mol. Struct. (Theochem)* **1998**, *423*, 101.
38. Mao, C.; Subeck, E. A.; Venkatachalam, T. K.; Uckun, F. M. *Biochem. Pharmacol.* **2000**, *60*, 1251.
39. The binding pocket of nevirapine was selected to study pyridinone–RT interactions because it is the structure with the highest resolution available and represent well the binding mode of the pyridinones within the binding geometries of 1051U91, 9-Cl-TIBO, Cl-α-APA, efavirenz, UC-781, and S-1153.
40. Parreira, R. L. T.; Abrahão, O.; Galembeck, S. E. *Tetrahedron* **2001**, *57*, 3243.
41. Tantillo, C.; Ding, J.; Jacobo-Molina, A.; Nanni, R. G.; Boyer, P. L.; Hughes, S. H.; Pauwels, R.; Andries, K.; Janseen, P. A. J.; Arnold, E. *J. Mol. Biol.* **1994**, *243*, 369.
42. Ren, J.; Nichols, C.; Bird, L.; Chamberlain, P.; Weaver, K.; Short, S.; Stuart, D. I.; Stammers, D. K. *J. Mol. Biol.* **2001**, *312*, 795.
43. Hopkins, A. L.; Ren, J.; Tanaka, H.; Baba, M.; Okamoto, M.; Stuart, D. I.; Stammers, D. K. *J. Med. Chem.* **1999**, *42*, 4500.
44. Sybyl version 6.8; Tripos, Inc., St. Louis, MO.
45. ViewerPro version 4.2; Accelrys, Inc, San Diego, CA.
46. Brookhaven Protein Data Bank. http://www.rcsb.org.
47. Weiner, S. J.; Kollman, P. A.; Case, D. A.; Singh, U. C.; Ghio, C.; Alagona, G.; Profeta, S.; Weiner, P. *J. Am. Chem. Soc.* **1984**, *106*, 765.
48. Gasteiger, J.; Marsili, M. *Tetrahedron* **1980**, *36*, 3219.
49. Mehler, E. L.; Solmajer, T. *Protein Eng.* **1991**, *4*, 903.
50. Streitwieser, A. *Molecular Orbital Theory for Organic Chemists*; Wiley: New York, 1961.
51. Clark, M.; Cramer, R. D., III; Van Opdenbosch, N. *J. Comput. Chem.* **1989**, *10*, 982.